AVIAN DISEASES 60:329–336, 2016

Spatial Modeling of Wild Bird Risk Factors for Highly Pathogenic A(H5N1) Avian Influenza Virus Transmission

Diann J. Prosser,[AJ] Laura L. Hungerford,[B] R. Michael Erwin,[C] Mary Ann Ottinger,[D] John Y. Takekawa,[EF] Scott H. Newman,[G] Xiangming Xiao,[H] and Erle C. Ellis[I]

[A]Patuxent Wildlife Research Center, U.S. Geological Survey, Beltsville, MD 20705
[B]University of Maryland School of Medicine, Baltimore, MD 21201
[C]Patuxent Wildlife Research Center, U.S. Geological Survey, Charlottesville, VA 22904
[D]Department of Biology and Biochemistry, University of Houston, Houston, TX 77204
[E]Western Ecological Research Center, U.S. Geological Survey, Vallejo, CA 94592
[F]National Audubon Society, Science Division, San Francisco, CA 94104
[G]Food and Agriculture Organization of the United Nations, Emergency Center for Transboundary Animal Diseases (ECTAD), Hanoi, Vietnam
[H]Center for Spatial Analysis, Department of Microbiology and Plant Biology, University of Oklahoma, Norman, OK 73019
[I]Department of Geography and Environmental Systems, University of Maryland Baltimore County, Baltimore, MD 21250

Received 13 May 2015; Accepted 2 November 2015; Published ahead of print 5 November 2015

SUMMARY. One of the longest-persisting avian influenza viruses in history, highly pathogenic avian influenza virus (HPAIV) A (H5N1), continues to evolve after 18 yr, advancing the threat of a global pandemic. Wild waterfowl (family Anatidae) are reported as secondary transmitters of HPAIV and primary reservoirs for low-pathogenic avian influenza viruses, yet spatial inputs for disease risk modeling for this group have been lacking. Using geographic information software and Monte Carlo simulations, we developed geospatial indices of waterfowl abundance at 1 and 30 km resolutions and for the breeding and wintering seasons for China, the epicenter of H5N1. Two spatial layers were developed: cumulative waterfowl abundance (W_{AB}), a measure of predicted abundance across species, and cumulative abundance weighted by H5N1 prevalence (W_{PR}), whereby abundance for each species was adjusted based on prevalence values and then totaled across species. Spatial patterns of the model output differed between seasons, with higher W_{AB} and W_{PR} in the northern and western regions of China for the breeding season and in the southeast for the wintering season. Uncertainty measures indicated highest error in southeastern China for both W_{AB} and W_{PR}. We also explored the effect of resampling waterfowl layers from 1 to 30 km resolution for multiscale risk modeling. Results indicated low average difference (less than 0.16 and 0.01 standard deviations for W_{AB} and W_{PR}, respectively), with greatest differences in the north for the breeding season and southeast for the wintering season. This work provides the first geospatial models of waterfowl abundance available for China. The indices provide important inputs for modeling disease transmission risk at the interface of poultry and wild birds. These models are easily adaptable, have broad utility to both disease and conservation needs, and will be available to the scientific community for advanced modeling applications.

RESUMEN. Modelo espacial de factores de riesgo de aves silvestres para la transmisión del virus de la influenza aviar de alta patogenicidad (H5N1).

Uno de los virus de la influenza aviar de más larga persistencia en la historia, es el virus de la influenza aviar A altamente patógeno (H5N1), que continúa evolucionando después de 18 años, este avance constituye una amenaza de pandemia mundial. Se ha reportado que las aves acuáticas silvestres (familia Anatidae) son transmisores secundarios de HPAIV y principales reservorios de virus de influenza aviar de baja patogenicidad. Los estudios de modelos espaciales para factores de riesgo de esta enfermedad son escasos. Mediante el uso de software de información geográfica y simulaciones tipo Monte Carlo, se desarrollaron índices geoespaciales para poblaciones abundantes de aves acuáticas con 1 y 30 km de resolución y para las estaciones de reproducción y de invierno para China, que son el epicentro del virus H5N1. Se desarrollaron dos capas espaciales: la abundancia de aves acuáticas acumulada (W_{AB}), una medida de la abundancia predicha a través de especies y una abundancia acumulativa ponderada por la prevalencia del virus H5N1 (W_{PR}), mediante el cual la abundancia de cada especie se ajustó con base a los valores de prevalencia y luego ascendió a través de las especies. Los patrones espaciales de la salida del modelo difirieron entre temporadas, con una mayor W_{AB} y W_{PR} en las regiones norte y oeste de China durante la época de reproducción y en el sureste de la temporada de invierno. Las medidas de incertidumbre indican mayor error en el sureste de China, tanto para W_{AB} y W_{PR}. También se exploró el efecto del re-muestreo de capas de aves acuáticas con resoluciones de 1 a 30 km para el modelo de riesgos de múltiples escalas. Los resultados indicaron una diferencia promedio baja (desviaciones estándar menores de 0.16 y 0.01 para W_{AB} y W_{PR}, respectivamente), con mayores diferencias en el norte para la época de reproducción y en el sureste para la temporada de invierno. Este trabajo proporciona los primeros modelos geoespaciales de abundancia de aves acuáticas disponibles para China. Los índices proporcionan información importante para establecer modelos para la transmisión de la enfermedad en la interface de la avicultura comercial y aves silvestres. Estos modelos son fácilmente adaptables, tienen amplia utilidad tanto para la enfermedad y para las necesidades de conservación y estarán a disposición de la comunidad científica para aplicaciones avanzadas de modelos.

Key words: H5N1, highly pathogenic avian influenza virus, spatial modeling, waterfowl, GIS

Abbreviations: GIS = geographic information software; HPAIV = highly pathogenic avian influenza virus; H5N1 = HPAIV A(H5N1)

[J]Corresponding author. E-mail: dprosser@usgs.gov

The persistence of highly pathogenic avian influenza virus (HPAIV) A (H5N1) (hereafter H5N1) and emergence of multiple new HPAIVs in Asia and the Americas A(H5N8, H5N2) in the last year brings the global community to a new level of concern over the avian influenza pandemic potential (17,35). Disease risk modeling can be an important tool for identifying areas with higher transmission potential, thereby allowing for strategic allocation of limited resources for disease surveillance and prevention. Wild waterfowl are known reservoirs for low-pathogenic avian influenza viruses (1). Following the evolution of H5N1 and H5N8, migratory waterfowl have become potential short-distance vectors for some HPAIVs (12,16,20,30), marking a new era of avian influenza viruses that pose increased threats to the economy and health of human, poultry, and wildlife populations. The interface of wild birds and poultry on the landscape is an important focal point for potential interspecies transmission and viral evolution. Development of risk models at this intersection has the potential to greatly benefit surveillance, pandemic preparedness, and prevention plans. Acquiring a spatial understanding of the distributions of high-risk populations is a critical first step in developing predictive disease transmission models; however, it is also one met with challenges due to poor availability of data (13,31).

In our efforts to model H5N1 transmission risk at the wild bird–poultry interface for China, we found that geospatial inputs were not readily available for either the wild bird or the poultry populations and therefore needed to be developed (32). We created high-resolution species-level gridded maps for domestic chickens, ducks, and geese of China by disaggregating county, prefecture, and provincial-level agricultural census data using a suite of remotely sensed environmental predictors (33). Creating seasonal distribution models for China's waterfowl required a different approach due to the large diversity of species (30 breeding and 37 wintering species), the variation in their natural ranges, and the inconsistency of data available for each. Step 1 involved development of predicted distributions (presence/absence) for each species and season resulting in a total of 42 1 km resolution gridded maps (31). Step 2 included (a) converting the distributions into gridded abundance maps for each species and (b) weighting the abundance estimates for each species by reported H5N1 prevalence values from the literature. The product of this second step was a critical input for mapping H5N1 transmission risk at the interface of wild and domestic birds for China (32).

In this paper, we outline the final steps taken to create H5N1 prevalence-weighted gridded waterfowl abundance maps for use in disease transmission models at the wild and domestic bird interface. This included acquiring population estimates and H5N1 prevalence values for each species, applying these in spatial format, and conducting Monte Carlo simulations to provide gridded output for uncertainty measures. We expect that the results from this work will benefit future modeling of disease transmission at the wild-domestic bird interface in new regions where HPAIV has extended its range. The final geospatial data layers will be made available to the scientific community on a USGS webpage (https://www.pwrc.usgs.gov/ai).

MATERIALS AND METHODS

Study area and scale. The geographic extent of the models produced for this study is the mainland portion of the People's Republic of China (hereafter China). China is the epicenter of H5N1 (23), H7N9 (8), H10N8 (34), and multiple other avian influenza viruses of human and economic concern. We focused our models on this region because of its importance to the emergence of new HPAI viruses.

Models were generated at 1 km spatial resolution (i.e., spatial output in a gridded format, with each grid box, or "cell" measuring 1 km per side), within two temporal seasons: the waterfowl breeding season (April to July) and wintering season (November to March). We also investigated the effects of scale on our model results, comparing output at 1 km resolution, which is the native format of our predictor data, and 30 km resolution, which was chosen for disease modeling and approximates the average county size within China.

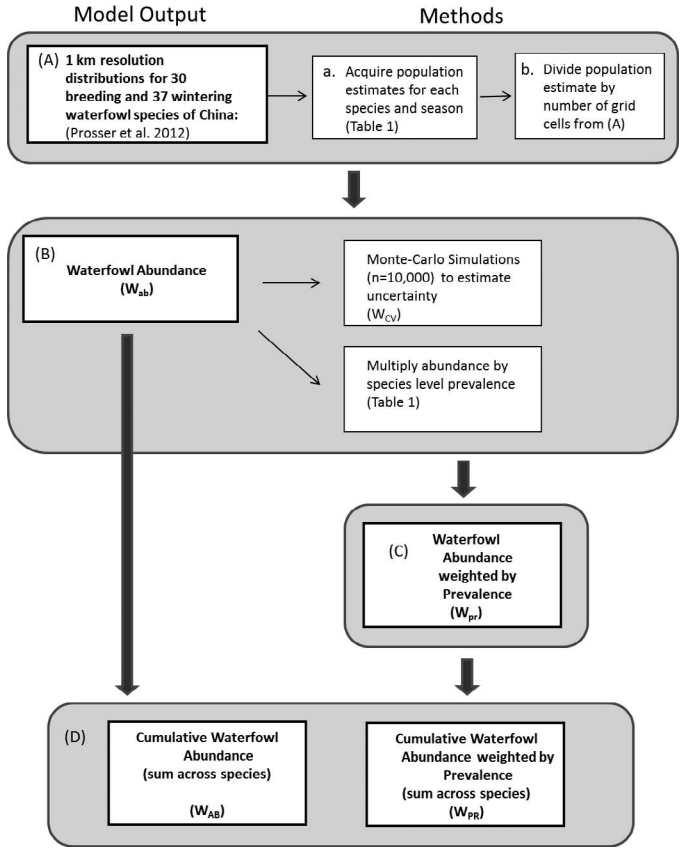

Fig. 1. Conceptual diagram of model production. (A) predicted presence distribution maps, (B) waterfowl abundance maps, and (C) abundance weighted by prevalence for China's 42 species of Anatidae waterfowl. Breeding and wintering season maps were produced for each product. (D) Cumulative W_{AB} and W_{PR} calculated by summing across species. Spatial resolution is 1 and 30 km grids.

Spatial modeling approach. We developed two indices to characterize densities of wild Anatidae waterfowl across the landscape: waterfowl abundance (W_{AB}) and abundance weighted by H5N1 prevalence (W_{PR}). Waterfowl abundance is a coarse prediction of the number of waterfowl (birds per cell). Waterfowl abundance weighted by prevalence is a proxy for the "effective" waterfowl population that may be shedding virus into the environment and potentially exposing susceptible birds to viruses (see basic SEIR compartmental disease models) (15,32).

The first step in the process was to develop distribution maps showing areas where a species was predicted to be present. These maps were developed using a habitat suitability approach (23,39) due to data restrictions for China's 42 waterfowl species (31). A database of waterfowl literature for China (Lee, unpublished; 31) was used to identify habitat requirements for each species. These requirements were then converted into equations that linked habitat to remotely sensed predictors including elevation and land cover (landsat.usgs.gov). The equations were applied using geographic information software (GIS) to identify cells across China where suitable habitat exists based on the remotely sensed predictors (31). Models were built separately for each species and season for a total of 30 breeding and 37 wintering species maps and are reported in Prosser *et al.* (29,31). In this paper, we expand upon the presence-absence distribution models to create abundance (W_{ab}) and H5N1 prevalence-weighted (W_{pr}), models for each species (Fig. 1). Cumulative waterfowl maps, designated as W_{AB} and W_{PR}, were created by summing across all species.

The W_{ab} models were created by dividing reported seasonal population estimates for China for a given species by the number of predicted presence grid cells and assigning that number to each cell in the distribution.

Population estimates for China were extracted from two leading references: Cao *et al.* (7), which reports population estimates for Anatidae wintering in the Yangtze River basin, and Delany and Scott (9), which reports global population estimates collated at the country level or broader regional levels. Since the majority of waterfowl winter in southeast China along the Yangtze River basin, we prioritized the Cao *et al.* (7) estimates when available; otherwise we deferred to Delany and Scott (9) (Table 1). Since waterfowl populations in Delany and Scott were often reported at regional scales greater than China, we estimated China populations by reducing the regional value by the proportion of the distribution range that falls outside of China. We placed confidence intervals around each estimate for use in uncertainty modeling, the latter estimates having much wider confidence bands than those extracted from Cao *et al.* (7) (see below). The resulting 1 km density distributions were summed across all species within a season to develop the cumulative W_{AB} spatial model.

In a similar fashion, we applied H5N1 prevalence values for each species (Table 1) to the abundance distributions to create an index of "effective" or potentially "virus shedding" population. Prevalence values were extracted from the literature for each species (Table 1). In cases where no data existed, prevalence was averaged across species within a taxonomic group (i.e., for ducks, geese, or swans) and used as an estimate for prevalence for a given species. Although we use the term H5N1 prevalence (defined as the proportion of a population determined positive for H5N1), we recognize that population-level sampling has not been achieved for most wild bird species (1,11,14,21,25,27). In addition, as viruses evolve over time, the reliability of detection rates will be dependent on the ability of labs to adapt protocols and assays to be sensitive to changing viruses. The prevalence-weighted abundance index was calculated by taking the product of a species' abundance and its prevalence value (Fig. 1B). For example, $W_{pr} = W_{ab} \times$ prevalence; with hypothetical inputs: $W_{pr} = 10$ birds $\times$ 0.05 prevalence $= 0.5$ effective birds with potential to shed virus. Cumulative prevalence-weighted abundance indices (W_{PR}) were developed by summing values across all species layers within a season, resulting in breeding and wintering season models. All analyses were conducted using ArcGIS 10.0 (ESRI, Redlands, CA) and Python (www.python.org).

We incorporated estimates of uncertainty for W_{ab} based on the wide range of confidence that we had for species-level estimates. We placed higher confidence on the population estimates published specifically for China, which were all wintering populations from Cao *et al.* (7) (21 of the 37 wintering species found in China); for these, we drew a 15% confidence band around each population estimate (Table 1). The remaining wintering estimates (16 species) and all of the breeding population estimates (30 species) were derived from global populations published in Delaney and Scott (9), who list population figures by region for the breeding and wintering seasons and provide country-level estimates where sufficient data were available. We derived estimates from the eastern Asia region, which included China, South Korea, Japan, Mongolia, and northeastern Russia. We drew wider confidence bands around these derived estimates, ranging from 15% to 90% (the majority ranging between 30% and 60%) depending on the size of the population and level of supporting data (5). We developed estimates of coefficient of variation (CV) for each species and season using triangular distributions in a Monte Carlo simulation with 10,000 runs (3). The population estimate was used as the best estimate, and high/low estimates calculated based on the confidence bands were used for the maximum and minimum limits of the triangular distribution (Table 1). CVs for the cumulative abundance distributions were expressed as the mean CV across all species (Fig. 1B). Monte Carlo simulations were run using program R, package mc2d (28,35).

Assessing differences in model scale. We examined the effects of resampling waterfowl abundance inputs from 1 to 30 km using a standard bilinear technique (10) whereby the distance-weighted average is calculated using the four nearest pixel values. This was done to examine the effects of scale differences of model inputs for the final wild-domestic bird interface transmission risk models (32), which model risk at both 1 and 30 km resolution. We considered 30 km grids because they approximate the average county size for China, which may be considered a more realistic scale for predicting transmission risk, even if poultry and wild waterfowl layers can be developed at 1 km resolution. Differences between the two scales of abundance maps were created by subtracting the 30 km grid cell values from the 1 km values and symbolizing in units of (a) no change, (b) change within 1 standard deviation of the mean, and (c) change greater than 1 standard deviation of the mean. These calculations were performed in ArcGIS 10.0 (ESRI, Redlands, CA).

RESULTS

Waterfowl abundance (W_{AB}), prevalence-weighted abundance (W_{PR}), and uncertainty. Waterfowl abundance maps, based on species-level seasonal distributions and reported population estimates, were created as an interim step toward developing H5N1 prevalence-weighted waterfowl abundance models (Fig. 1B). We created 1 km gridded rasters for each species and season (breeding and wintering) for species abundance, H5N1 prevalence, and coefficient of variation (uncertainty for abundance metric). Patterns of wintering and breeding W_{ab} differed by species (Fig. 2) as did prevalence values from the literature (Fig. 2; Table 1). We provide a visual example for two species of high importance to H5N1 transmission: the bar-headed goose (*Anser indicus*) and mallard (*Anas platyrhynchos*) (Fig. 2). W_{ab} for the bar-headed goose was 0.31 birds per cell in the breeding season versus 0.06 for the winter. The mallard had 1.46 and 0.05 abundance estimates per cell for breeding and wintering, respectively. The prevalence values were 2.3 for the bar-headed goose and 11.2 for the mallard (21). CV between the seasons and species ranged from 0.03 to 0.13. In general, both species had predicted wintering areas in southeastern China; however, the range of the bar-headed goose was much more restricted than the ubiquitous mallard. For breeding, the bar-headed goose range was restricted mainly to the high-elevation western Qinghai-Tibetan Plateau, and the mallard had a predicted range across parts of the Plateau as well as the wetland-dominated regions of northeastern China.

Species-specific H5N1 prevalence values from samples taken within China (21) were available for 9 of the 42 species (Table 1). For the remaining species, we estimated prevalence under the following conditions: for 11 species, we calculated prevalence as the average across the available global literature (11,14,25,27); and for the remaining 22 species that had no species-level prevalence values in the literature, we used the average per taxonomic group from Kou *et al.* (21): 1.4 for geese, 5.3 for dabbling ducks, and 5.0 for diving ducks, respectively.

Cumulative waterfowl abundance estimates ranged from zero to 5.0 birds per cell for the breeding season and zero to 7.9 for the wintering season with mean values of 0.07 and 0.08 across China (Fig. 3, middle panels). Patterns of total waterfowl abundance were highest in northeastern China and across the southeastern portions of the Qinghai-Tibetan Plateau (western China).

Mean cumulative waterfowl abundance weighted by prevalence was higher for the breeding versus wintering season (average of 0.01 versus 0.006 birds across all grid cells of China), although maximum values were 0.32 and 0.39, respectively (Fig. 3, top panels). W_{PR} patterns were highest across most of China for the breeding season and mainly in the southeast for the wintering season; however, on a local scale, the breeding season patterns were more tightly clustered in local patches. The areas with highest W_{PR} estimates for the breeding season were similar to the abundance patterns, with high values on the Plateau and in the northeast.

The average coefficient of variation for abundance was 0.19 and 0.11 for the breeding and wintering seasons. The highest CV values were located in the lowland regions of southeastern China, for both the breeding and wintering seasons (Fig. 3, bottom panels).

Effects of scale. Investigation of the effect of resampling the abundance- (W_{AB}) and prevalence-weighted layers (W_{PR}) from 1 to 30 km spatial resolution indicated the greatest differences in the northeast for

Table 1. Species name, code, population estimates, and H5N1 prevalence rates for China's 42 Anatidae waterfowl species.

Mcode[A]	Common name	Scientific name	Winter population	Winter low	Winter high	Summer population[B]	Summer low[C]	Summer high[C]	H5N1 prevalence	Abun Br[D]	Abun Wi[D]
M064	Lesser Whistling Duck	*Dendrocygna javanica*	1500[B]	1000	2000	15,000	5000	25,000	5.3[G]	0.10	0.01
M066	Mute Swan	*Cygnus olor*	0	0	0	650	300	1000	3.4[F]	0	0
M067	Whooper Swan	*Cygnus cygnus*	5900[C]	5015	6785	300	100	500	4.0[F]	0	0.01
M068	Tundra Swan	*Cygnus columbianus*	81,000[C]	68,850	93,150	0	0	0	2.8[F]	0	0.13
M069	Swan Goose	*Anser cygnoides*	78,000[C]	66,300	89,700	40,000	30,000	50,000	1.4[G]	0.22	0.16
M070	Bean Goose	*Anser fabalis*	150,000[C]	127,500	172,500	0	0	0	0.0[F]	0	0.23
M071	Greater White-fronted Goose	*Anser albifrons*	33,000[C]	28,050	37,950	0	0	0	2.2[F]	0	0.04
M072	Lesser White-fronted Goose	*Anser erythropus*	21,000[C]	17,850	24,150	0	0	0	2.1[E]	0	0.03
M073	Greylag Goose	*Anser anser*	40,000[B]	15,000	65,000	40,000	15,000	65,000	0.8[E]	0.12	0.02
M074	Bar-headed Goose	*Anser indicus*	15,000[B]	10,000	20,000	56,000	52,000	60,000	2.3[E]	0.31	0.06
M075	Snow Goose	*Anser caerulescens*	50[B]	25	75	0	0	0	1.4[G]	0	0
M077	Brent Goose	*Branta bernicla*	0	0	0	0	0	0	1.0[E]	0	0
M079	Ruddy Shelduck	*Tadorna ferruginea*	15,000[B]	10,000	20,000	19,000	13,000	25,000	2.2[F]	0.04	0.02
M081	Common Shelduck	*Tadorna tadorna*	18,000[C]	15,300	20,700	12,000	9000	15,000	3.6[F]	0.06	0.08
M083	Cotton Pygmy Goose	*Nettapus coromandelianus*	200[B]	100	300	15,000	5000	25,000	5.3[G]	0.01	0
M084	Mandarin Duck	*Aix galericulata*	20,000[B]	10,000	30,000	6000	4000	8000	5.3[G]	0.17	0.02
M085	Gadwall	*Anas strepera*	7700[C]	6545	8855	14,000	10,000	18,000	2.1[F]	0.07	0.03
M086	Falcated Duck	*Anas falcate*	78,000[C]	66,300	89,700	17,000	10,000	24,000	5.3[G]	0.12	0.07
M087	Eurasian Wigeon	*Anas penelope*	50,000[C]	42,500	57,500	37,000	25,000	50,000	1.9[E]	0.33	0.04
M089	Mallard	*Anas platyrhynchos*	73,000[C]	62,050	83,950	575,000	375,000	750,000	11.2[F]	1.46	0.05
M090	Spot-billed Duck	*Anas poecilorhyncha*	100,000[C]	85,000	115,000	450,000	300,000	600,000	3.7[F]	0.31	0.21
M092	Northern Shoveler	*Anas clypeata*	27,000[C]	22,950	31,050	40,000	30,000	50,000	10.2[E]	0.37	0.10
M093	Northern Pintail	*Anas acuta*	46,000[C]	39,100	52,900	2000	1000	3000	9.8[E]	0.20	0.23
M094	Garganey	*Anas querquedula*	50,000[B]	30,000	70,000	30,000	20,000	40,000	5.3[G]	0.18	0.14
M095	Baikal Teal	*Anas formosa*	91,000[C]	77,350	104,650	0	0	0	5.3[G]	0	0.35
M096	Common Teal	*Anas crecca*	146,000[C]	124,100	167,900	80,000	60,000	100,000	3.1[E]	0.56	0.36
M097	Marbled Duck	*Marmaronetta angustirostris*	0	0	0	1500	100	2900	5.0[G]	0.43	0
M098	Red-crested Pochard	*Rhodonessa rufina*	0	0	0	1000	500	1500	2.9[E]	0.02	0
M099	Common Pochard	*Aythya ferina*	18,000[C]	15,300	20,700	500	100	900	5.0[G]	0.07	0.08
M101	Ferruginous Pochard	*Aythya nyroca*	5000[B]	2000	8000	5000	2000	8000	5.0[G]	0.07	0.09
M102	Baer's Pochard	*Aythya baeri*	850[C]	723	978	1500	1000	2000	5.0[G]	0.01	0
M103	Tufted Duck	*Aythya fuligula*	11,000[C]	9350	12,650	1000	500	1500	7.1[F]	0.01	0.05
M104	Greater Scaup	*Aythya marila*	80,000[B]	60,000	100,000	0	0	0	5.0[G]	0	0.80
M105	Steller's Eider	*Polysticta stelleri*	0	0	0	0	0	0	5.0[G]	0	0.80
M107	Long-tailed Duck	*Clangula hyemalis*	30,000[B]	20,000	40,000	0	0	0	5.0[G]	0	0.52
M108	Black Scoter	*Melanitta nigra*	40,000[B]	20,000	60,000	0	0	0	5.0[G]	0	3.08
M109	White-winged Scoter	*Melanitta fusca*	40,000[B]	20,000	60,000	0	0	0	5.0[G]	0	0.83
M110	Common Goldeneye	*Bucephala clangula*	20,000[B]	10,000	30,000	1000	500	1500	5.0[G]	0.15	0.07
M111	Smew	*Mergellus albellus*	15,000[C]	12,750	17,250	200	100	300	5.0[G]	0.20	0.04
M112	Red-breasted Merganser	*Mergus serrator*	3500[B]	2000	5000	200	100	300	5.0[G]	0.05	0.02
M113	Scaly-sided Merganser	*Mergus squamatus*	200[B]	100	300	100	50	150	5.0[G]	0.03	0
M114	Common Merganser	*Mergus merganser*	29,000[C]	24,650	33,350	10,000	7000	13,000	5.0[G]	0.68	0.08

[A]Mcode refers to the reference map code in Ref. (22).
[B]Population estimates are based on Ref. (7).
[C]Population estimates are based on Ref. (9).
[D]Abun Br = per cell abundance estimate for the breeding season; Abun Wi = per cell abundance estimate for the wintering season.
[E]Prevalence values are from Ref. (21).
[F]Prevalence values are an average of Refs. (11,14,25,27).
[G]Averages for swans, geese, or ducks are from Ref. (21).

the breeding season and in the southeast for the wintering season (Fig. 4). The average difference across all grid cells was 0.155 and 0.152 for the breeding and wintering W_{AB} indices and 0.01 and 0.006, respectively for the W_{PR} indices.

DISCUSSION

The main objective of this study was to develop high-resolution spatial inputs for wild bird populations for H5N1 risk modeling at

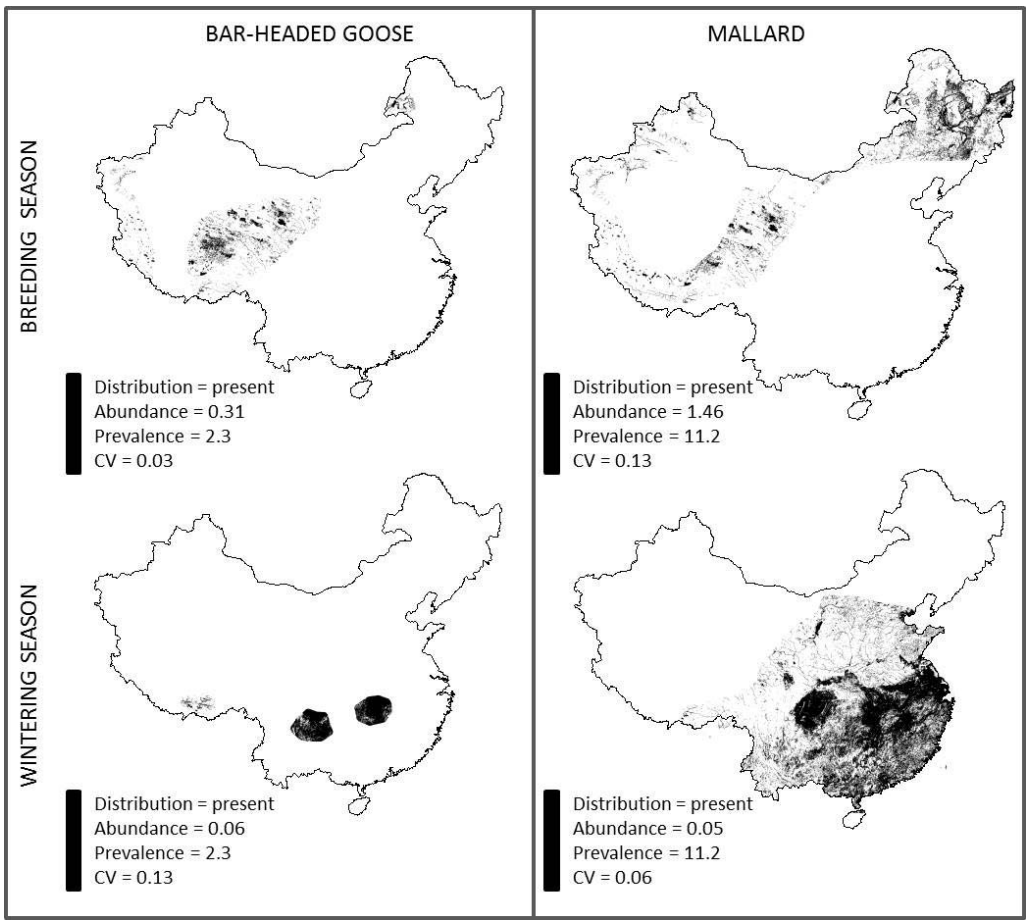

Fig. 2. Species-level distribution maps for two example waterfowl species (bar-headed goose and mallard). Upper panels represent breeding season, lower panels represent wintering season. Legends represent values for four separate outputs: (1) presence-absence distributions, (2) abundance estimates (birds per cell), (3) prevalence (cumulative sum of species abundances multiplied by species or group H5N1 prevalence values from the literature), and (4) CV (standard deviation divided by mean) for the abundance estimate.

the interface of wild and domestic birds—first, by developing abundance models for China's wintering and breeding waterfowl species, and, second, by weighting these abundance maps by species-specific H5N1 prevalence. Weighting of the species abundance maps by H5N1 prevalence was an important step for the risk modeling (32) because even though waterfowl are reservoirs for low pathogenic avian influenza viruses (2), their susceptibility to HPAIV H5N1 and ability to shed virus differs among species (4,6,18,36,37). The difference in pattern between breeding and wintering seasons when examining local scale differences between W_{AB} and W_{PR} indicated that adding prevalence to the waterfowl abundance layer is effective in capturing complexity between these two variables at the species level.

One interesting difference between the W_{AB} and W_{PR} layers was a large-scale similarity in pattern for the breeding season, but regional differences for the wintering season. For example, local areas on the southern Qinghai-Tibetan Plateau (near Lhasa, Tibet) and in southwestern China (Yunnan Province) showed moderate values for W_{AB} and maximum values for W_{PR}, after the species-level prevalence values were incorporated. This indicates complexity and variation in the combination of waterfowl abundance and prevalence at the species level.

Uncertainty measures from the Monte Carlo simulations showed consistent and interesting patterns between seasons (Fig. 3, bottom panel). Regions with high mean CVs tended to be concentrated in the southeastern part of China, for both the breeding and wintering models. This pattern was expected for the wintering species, since the majority of China's wintering waterfowl population is found in this region (7); however, it was a surprising result for the breeding species, which are generally located in the north and high elevation western parts of China. In the case of the breeding models, CVs were high (>0.5) for two groups of waterfowl: (1) uncommon breeders within China including two swan species (mute and whooper swans: *Cygnus olor* and *Cygnus cygnus*) and diving ducks (pochards, goldeneyes, and mergansers: *Rhodonessa, Aythya, Bucephala,* and *Mergus* spp.), and (2) two tropical breeding duck species (lesser whistling duck and cotton-pygmy goose: *Dendrocygna javanica* and *Nettapus coromandelianus*). The concentration of high CV values in southeastern China was driven by the tropical species, which tend to have wide distributions and large confidence intervals surrounding the population estimates. As expected, the mean CV (across all grid cells of China) was higher for the breeding season than the wintering season because of the associated less-certain population estimates (Table 1). Including a measure of uncertainty in the abundance models gives us a mechanism to address the species-level differences in confidence in population estimates.

Two main data sources were used to derive population estimates for China: Cao *et al.* (7) and Delany and Scott (9). More recent publications for this area from 2012 report on range contractions or decreases in population estimates for certain species of concern. For example, Wang *et al.* (40) reports a decrease in lesser white-fronted geese during the period 2002 through 2011 (approximately 21,000 birds). This estimate is the same as the one originally derived from Delany and Scott (9). Since the paper suggests incomplete coverage

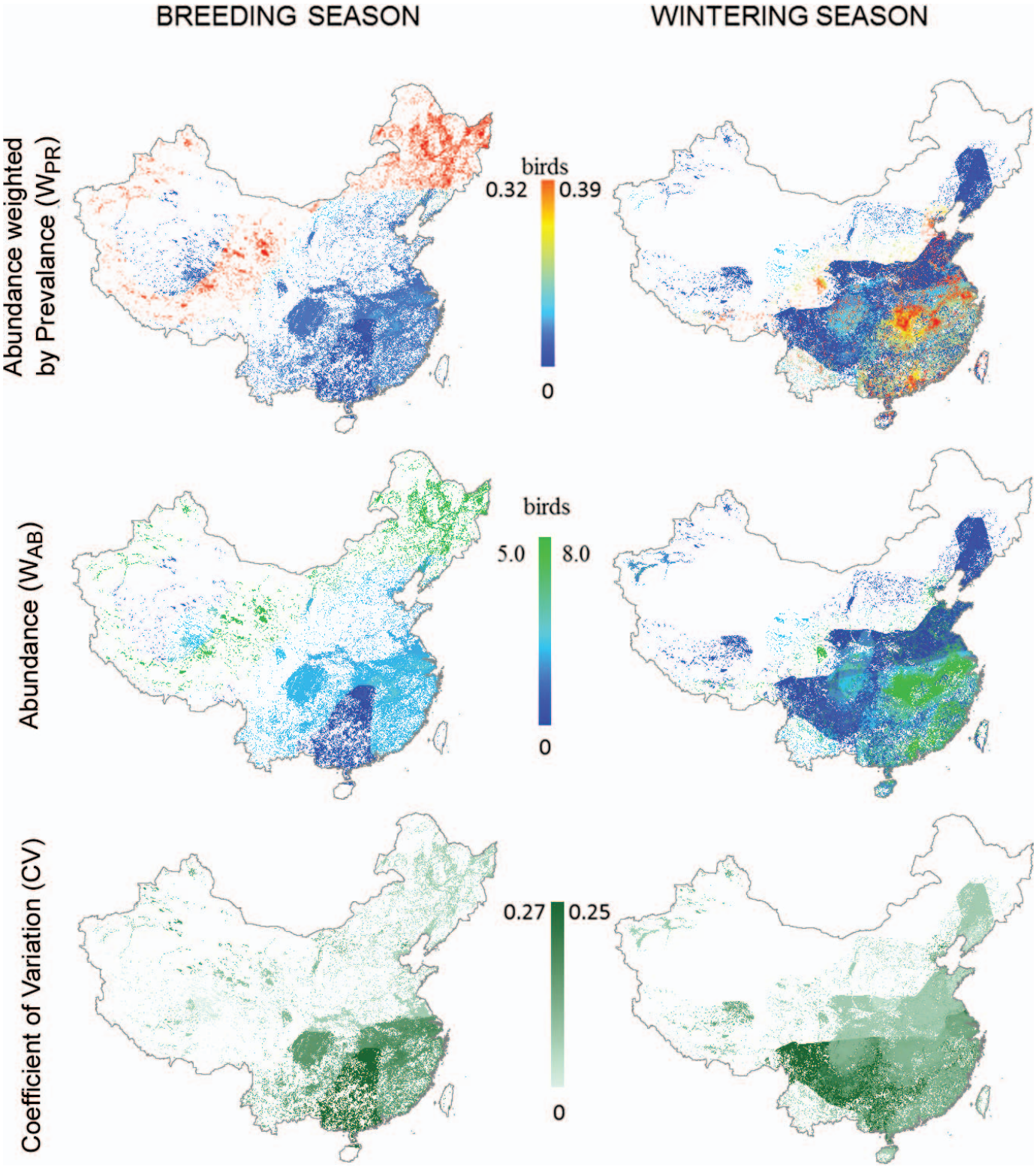

Fig. 3. Index of abundance weighted by prevalence (W_{PR}), abundance (W_{AB}), and coefficient of variation (CV) for China's 42 Anatidae waterfowl species. Left panel represents breeding season (approximately April through July); right panel represents wintering season (approximately November through March). Units are birds per km^2 (W_{PR} and W_{AB}).

of the Yangtze River basin, we did not change the estimate nor did we change from the wider confidence band associated to the narrower ones used for targeted population estimates for China. A second paper published by Wang *et al.* (39) reported range contraction and varying max counts for the period of 2002 through 2012 (2131 individuals) and an all-time low max count of 194 birds in 2012. The authors suggest coordinated surveys in the Dongting Reserve (an important wintering site) and along the Yangtze River basin.

Reasons for the declining populations and shrinking ranges of the aforementioned species included anthropogenic pressures such

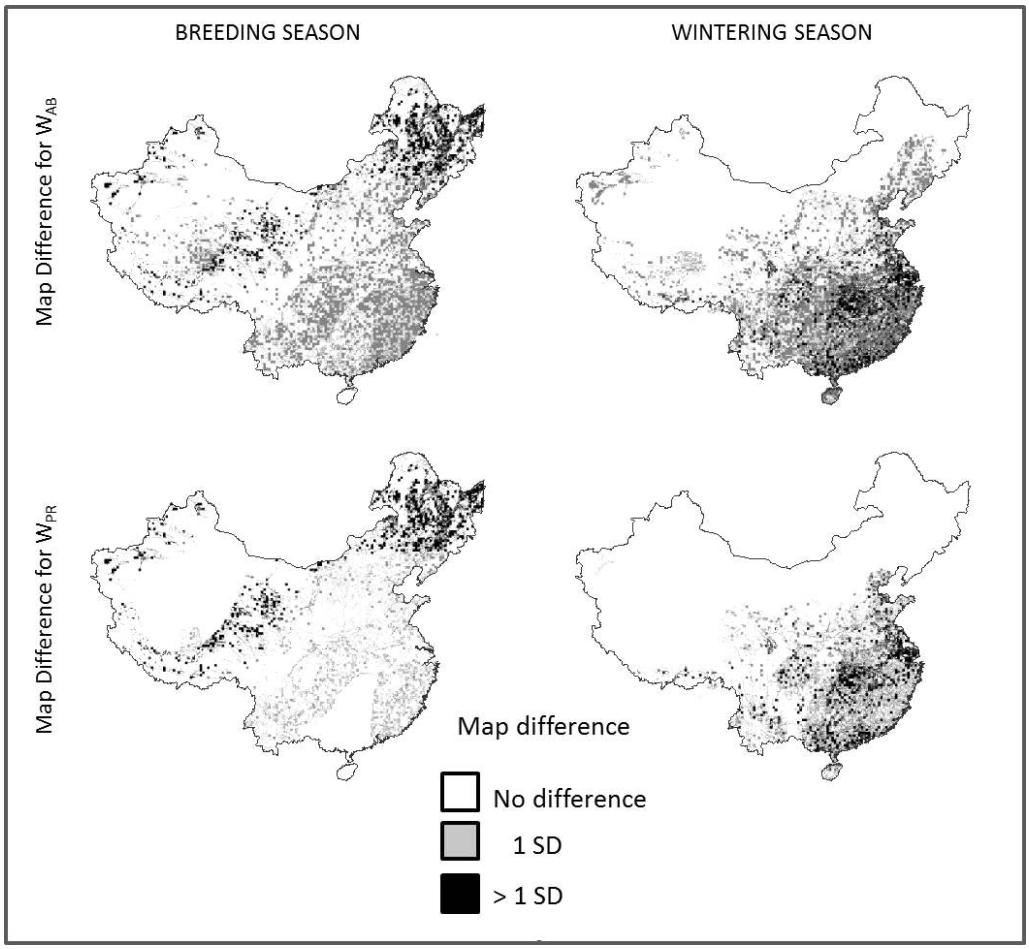

Fig. 4. Map difference between 1 and 30 km resolution maps visualized in standard deviations from the mean for waterfowl abundance (top panel) and H5N1 prevalence estimates. Left panel is breeding season, right panel is wintering season.

as hunting, habitat loss, and wetland degradation due to decreasing water levels (39,40). A changing landscape may force wild species to seek new areas for refuge and fueling, squeezing them into suboptimal habitat that could decrease the fitness of individuals, as well as forcing them closer to human and agricultural settings. As wild birds increase their usage of anthropogenic habitats, the interface between domestic and wild birds increases with potential implications to frequency of virus transmission among populations.

One step in the modeling process that may not be biologically relevant is the equal distribution of population estimates across the total number of predicted presence grid cells (Fig. 1A and 1B). Most waterfowl species defend territories during the breeding season; however, a few species such as the bar-headed goose nest in loose colonies (19). We would expect a more clustered pattern in real-world nesting distributions for such species; however, we do not have a good source of data to model this. Similarly, during winter, waterfowl are gregarious in nature and do not form territories (19). The habitat requirement equations developed as part of the predicted presence distribution modeling (31) may naturally reflect the habitat differences between breeding and wintering seasons; however, in reality, waterfowl are not distributed equally across all suitable habitat. We proceeded with this approach because the data we have available are not rigorous enough to develop finer predictions.

We investigated the effect of resampling the W_{AB} and W_{PR} from 1 to 30 km spatial resolution to determine what effect this might have as inputs to the overall risk modeling. The largest differences due to resampling occurred in the northeast for the breeding season and in the southeast for the wintering season (Fig. 4), as we might expect, given that these were the areas with highest abundance and weighted prevalence values. Bilinear interpolation uses a weighted average to calculate a resampled value based on the four nearest input cells. High values within grid cells at the 1 km resolution layers surrounded by zero value grid cells would produce the larger differences when interpolated across scales.

Here we provide high-resolution gridded spatial maps of predicted waterfowl abundance and abundance weighted by H5N1 prevalence for inclusion in disease transmission models at the wild-domestic bird interface. These models are critical inputs for the risk modeling that did not previously exist. The waterfowl abundance models can have broad utility beyond disease applications. This suite of models has been developed across species and seasons, with accompanying layers that quantify the uncertainty within the population estimates.

REFERENCES

1. Alexander, D. J. A review of avian influenza in different bird species. Vet. Microbiol. 74:3–13. 2000.

2. Alexander, D. J. Summary of avian influenza activity in Europe, Asia, and Australasia, 2002–2006. Avian Dis. 51:161–166. 2007.

3. Beale, C. M., and J. J. Lennon. Incorporating uncertainty in predictive species distribution modelling. Philos. Trans. R. Soc. Lond. B. Biol. Sci. 367:247–58. 2012.

4. Brown, J. D., D. E. Stallknecht, and D. E. Swayne. Experimental infection of swans and geese with highly pathogenic avian influenza virus (H5N1) of Asian lineage. Emerg. Infect. Dis. 14:136–142. 2008.

5. Burmaster, D. E., and P. D. Anderson. Principles of good practice for the use of Monte Carlo Techniques in human health and ecological risk assessments. Risk Anal. 14:477–481. 1994.

6. Cagle, C., J. Wasilenko, S. C. Adams, C. J. Cardona, T. L. To, T. Nguyen, E. Spackman, D. L. Suarez, D. Smith, E. Shepherd, J. Roth, M. J. Pantin-Jackwood, M. J. Pantin, A. J. Wasilenko, A. S. C. Adams, B. C. J. Cardona, C. T. L. To, D. T. Nguyen, D. E. Spackman, A. D. Smith, A. E. Shepherd, A. J. Roth, and M. J. P. Ae. Differences in pathogenicity, response to vaccination, and innate immune responses in different types of ducks infected with a virulent H5N1 highly pathogenic avian influenza virus from Vietnam. Avian Dis. 56:479–487. 2012.

7. Cao, L., M. Barter, and G. Lei. New Anatidae population estimates for eastern China: implications for current flyway estimates. Biol. Conserv. 141:2301–2309. 2008.

8. Chen, E., Y. Chen, L. Fu, Z. Chen, Z. Gong, H. Mao, D. Wang, M. Y. Ni, P. Wu, Z. Yu, T. He, Z. Li, J. Gao, and S. Liu. Human infection with avian influenza A(H7N9) virus re-emerges in China in winter 2013. Eurosurveillance 18:7–14. 2013.

9. Delany, S., and D. Scott. Waterbird population estimates. Wetlands International, Wageningen, the Netherlands. 2006.

10. De Smith, Michael J., M. F. Goodchild, and P. Longley. Geospatial analysis: a comprehensive guide to principles, techniques and software tools. Troubador Publishing Ltd. 2007.

11. Gaidet, N., T. Dodman, and A. Caron. Influenza surveillance in wild birds in Eastern Europe, the Middle East, and Africa: preliminary results from an ongoing FAO-led survey. J. Wildl. Dis. 43:22–28. 2007.

12. Gilbert, M., S. H. Newman, J. Y. Takekawa, L. Loth, C. Biradar, D. J. Prosser, S. Balachandran, M. V. Subba Rao, T. Mundkur, B. Yan, Z. Xing, Y. Hou, N. Batbayar, T. Natsagdori, L. Hogerwerf, J. Slingenbergh, and X. Xiao. Flying over an infected landscape: distribution of highly pathogenic avian influenza H5N1 risk in south Asia and satellite tracking of wild waterfowl. Ecohealth 7:448–458. 2010.

13. Gilbert, M., and D. U. Pfeiffer. Risk factor modelling of the spatio-temporal patterns of highly pathogenic avian influenza (HPAIV) H5N1: a review. Spat. Spatio-temp. Epidemiol. 3:173–183. 2013.

14. Hesterberg, U., K. Harris, D. Stroud, V. Guberti, L. Busani, M. Pittman, V. Piazza, A. Cook, and I. Brown. Avian influenza surveillance in wild birds in the European Union in 2006. Influenza Other Resp. Viruses 3:1–14. 2009.

15. Hethcote, H. W. Three basic epidemiological models. In: Applied mathematical ecology, Volume 18. S. Levin, T. Hallam, and L. Gross, eds. Springer, Berlin Hiedelberg. pp. 119–144. 1989.

16. Jeong, J., H.-M. Kang, E.-K. Lee, B.-M. Song, Y.-K. Kwon, H.-R. Kim, K.-S. Choi, J.-Y. Kim, H.-J. Lee, O.-K. Moon, W. Jeong, J. Choi, J.-H. Baek, Y.-S. Joo, Y. H. Park, H.-S. Lee, and Y.-J. Lee. Highly pathogenic avian influenza virus (H5N8) in domestic poultry and its relationship with migratory birds in South Korea during 2014. Vet. Microbiol. 173:249–257. 2014.

17. Jhung, M., and D. Nelson. Outbreaks of avian influenza A (H5N2), (H5N8), and (H5N1) among birds—United States, December 2014–January 2015. MMWR Morb. Mortal. Wkly. Rep. 64:111. 2015.

18. Kalthoff, D., A. Breithaupt, J. P. Teifke, A. Globig, T. Harder, T. C. Mettenleiter, and M. Beer. Highly pathogenic avian influenza virus (H5N1) in experimentally infected adult mute swans. Emerg. Infect. Dis. 14:1267–1270. 2008.

19. Kear, J. Ducks, geese, and swans. Volume 2: Species accounts (Cairnina to Mergus). Oxford University Press, New York. 2005.

20. Keawcharoen, J., D. van Riel, G. van Amerongen, T. Bestebroer, W. E. Beyer, R. van Lavieren, A. D. M. E. Osterhaus, R. A. M. Fouchier, and T. Kuiken. Wild ducks as long-distance vectors of highly pathogenic avian influenza virus (H5N1). Emerg. Infect. Dis. 14:600–607. 2008.

21. Kou, Z., Y. Li, Z. Yin, S. Guo, M. Wang, X. Gao, P. Li, L. Tang, P. Jiang, Z. Luo, Z. Xin, C. Ding, Y. He, Z. Ren, P. Cui, H. Zhao, Z. Zhang, S. Tang, B. Yan, F. Lei, and T. Li. The survey of H5N1 flu virus in wild birds in 14 provinces of China from 2004 to 2007. PLoS ONE 4:e6926. 2009.

22. MacKinnon, J. R., and K. Phillipps. A field guide to the birds of China. Oxford University Press. 586 pp. 2000.

23. Morrison, M. L., B. G. Marcot, and R. Mannan. Wildlife-habitat relationships: concepts and applications, 3rd ed. University of Wisconsin Press, Madison. 2006.

24. Mukhtar, M. M., S. T. Rasool, D. Song, C. Zhu, Q. Hao, Y. Zhu, and J. Wu. Origin of highly pathogenic H5N1 avian influenza virus in China and genetic characterization of donor and recipient viruses. J. Gen. Virol. 88:1–3. 2007.

25. Munster, V. J., C. Baas, P. Lexmond, J. Waldenstrom, A. Wallensten, T. Fransson, G. F. Rimmelzwaan, W. E. P. Beyer, M. Schutten, B. Olsen, A. D. M. E. Osterhaus, and R. A. Fouchier. Spatial, temporal, and species variation in prevalence of influenza A viruses in wild migratory birds. PLoS Pathog. 3:1–9. 2007.

26. [OIE] World Organisation for Animal Health. Update on highly pathogenic avian influenza in animals: type H5 and H7. Available from: http://www.oie.int/animal-health-in-the-world/update-on-avian-influenza/2015/. OIE. 2015.

27. Olsen, B., V. J. Munster, A. Wallensten, J. Waldenström, A. D. M. E. Osterhaus, R. A. M. Fouchier, and J. Waldenstro. Global patterns of influenza A virus in wild birds. Science 312:384–388. 2006.

28. Pouillot, R., M. L. Delingnette-Muller, D. L. Kelly, and J. B. Denis. The mc2d package. Available from: http://riskassessment.r-forge.r-project.org/ 2010.

29. Prosser, D. J. Wild birds and emerging diseases: modeling avian influenza transmission risk between domestic and wild birds in China. Doctoral Dissertation. Univ. Maryland, College Park, MD. 2012.

30. Prosser, D. J., P. Cui, J. Y. Takekawa, M. Tang, Y. Hou, B. M. Collins, B. Yan, N. J. Hill, T. Li, Y. Li, F. Lei, S. Guo, Z. Xing, Y. He, Y. Zhou, D. C. Douglas, W. M. Perry, and S. H. Newman. Wild bird migration across the Qinghai-Tibetan plateau: a transmission route for highly pathogenic H5N1. PLoS ONE 6:e17622. 2011.

31. Prosser, D. J., C. Ding, R. M. Erwin, T. Mundkar, and E. C. Ellis. Species distribution modeling in a region of high need and limited data: China's Anatidae waterfowl. PLoS ONE. *In Review*. 2015.

32. Prosser, D. J., L. L. Hungerford, R. M. Erwin, M. A. Ottinger, J. Y. Takekawa, and E. C. Ellis. Mapping avian influenza transmission risk at the interface of domestic poultry and wild birds. Front. Public Health 1; article 28. 2013. [Internet; accessed 13th January 2015]. Available from: http://doi.org/10.3389/fpubh.2013.00028

33. Prosser, D. J., J. Wu, E. C. Ellis, F. Gale, T. P. Van Boeckel, W. Wint, T. Robinson, X. Xiao, and M. Gilbert. Modelling the distribution of chickens, ducks, and geese in China. Agric. Ecosyst. Environ. 141:381–389. 2011.

34. Qi, W., X. Zhou, W. Shi, L. Huang, W. Xia, D. Liu, H. Li, S. Chen, F. Lei, L. Cao, J. Wu, F. He, W. Song, Q. Li, M. Liao, and M. Liu. Genesis of the novel human-infecting influenza A(H10N8) virus and potential genetic diversity of the virus in poultry, China. Euro Surveill. 19:1–13. 2014.

35. R Core Development Team. R: a language and environment for statistical computing. R Foundation for Statistical Computing, Vienna, Austria. 2015.

36. Tang, Y., P. Wu, D. Peng, X. Wang, H. Wan, P. Zhang, J. Long, W. Zhang, Y. Li, W. Wang, X. Zhang, and X. Liu. Characterization of duck H5N1 influenza viruses with differing pathogenicity in mallard (*Anas platyrhynchos*) ducks. Avian Pathol. 38:457–67. 2009.

37. Tolf, C., N. Latorre-Margalef, M. Wille, D. Bengtsson, G. Gunnarsson, J. Elmberg, J. Waldenstro, V. Grosbois, D. Hasselquist, B. Olsen, and J. Waldenström. Individual variation in influenza A virus infection histories and long-term immune responses in mallards. PLoS ONE 8:1–9. 2013.

38. Verner, J., M. L. Morrison, and C. J. Ralph. Wildlife 2000: Modeling habitat relationships of terrestrial vertebrates. University of Wisconsin Press, Madison. 1986.

39. Wang, X., M. Barter, L. Cao, J. Lei, and A. D. Fox. Serious contractions in wintering distribution and decline in abundance of Baer's Pochard *Aythya baeri*. Bird Conserv. Int. 22:121–127. 2012.

40. Wang, X., A. D. Fox, P. Cong, M. Barter, and L. Cao. Changes in the distribution and abundance of wintering Lesser White-fronted Geese *Anser erythropus* in eastern China. Bird Conserv. Int. 22:128–134. 2012.

ACKNOWLEDGMENTS

This study was supported by funding from the United States Geological Survey Wild Bird Avian Influenza Program. We thank Ruth DeFries of Columbia University for expertise in remote sensing, and two anonymous reviewers for strengthening earlier versions of this paper. The use of trade, product, or firm names in this publication is for descriptive purposes only and does not imply endorsement by the U.S. government or FAO.